Vid2CAD: CAD Model Alignment using Multi-View Constraints from Videos

Kevis-Kokitsi Maninis[1,*] Stefan Popov[1,*] Matthias Nießner[2] Vittorio Ferrari[1]
[1]Google Research [2]Technical University of Munich

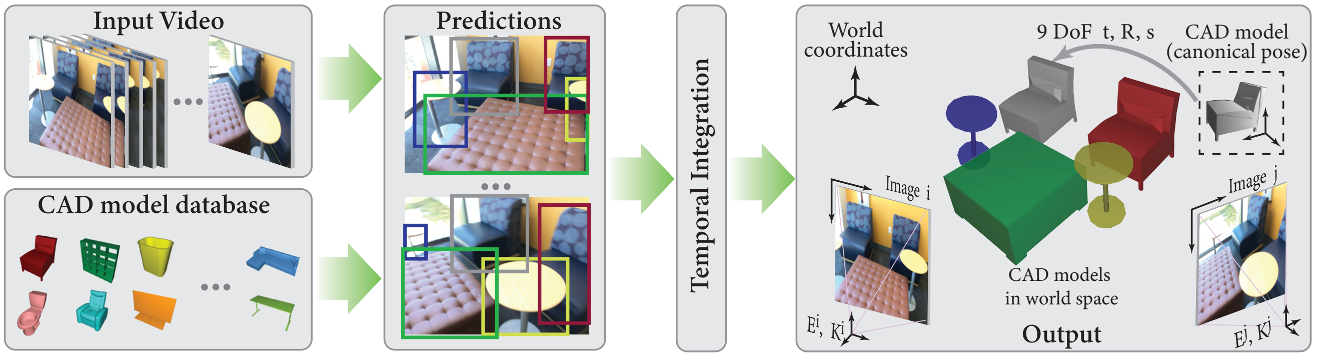

Figure 1: **Method overview**: given an RGB video sequence, the goal of our method is to find and align a CAD model from a database for each object in the scene. The objective is to find the transformations t, R, and s that moves each object from its canonical pose to the 3D world coordinate system of the 3D scene. The main idea of our approach is to integrate per-frame neural network predictions with a joint optimization formulation incorporating multi-view constraints. As a result, we obtain a clean, globally-consistent 3D CAD representation of all objects in the scene (right).

Abstract

We address the task of aligning CAD models to a video sequence of a complex scene containing multiple objects. Our method is able to process arbitrary videos and fully automatically recover the 9 DoF pose for each object appearing in it, thus aligning them in a common 3D coordinate frame. The core idea of our method is to integrate neural network predictions from individual frames with a temporally global, multi-view constraint optimization formulation. This integration process resolves the scale and depth ambiguities in the per-frame predictions, and generally improves the estimate of all pose parameters. By leveraging multi-view constraints, our method also resolves occlusions and handles objects that are out of view in individual frames, thus reconstructing all objects into a single globally consistent CAD representation of the scene. In comparison to the state-of-the-art single-frame method Mask2CAD that we build on, we achieve substantial improvements on Scan2CAD (from 11.6% to 30.2% class average accuracy)[1].

1. Introduction

Understanding real-world environments using visual data is at the heart of the computer vision community and it is a key requirement for many applications ranging from robotics to AR/VR scenarios. With the advent of scalable deep learning methods, we have seen significant progress towards these goals with impressive results on 2D images, including image classification [18, 37, 14], segmentation [24, 4], and detection methods [11, 34, 13]. In addition, we have seen promising works towards 3D understanding, for example 3D object reconstruction from a single RGB image using learnt data-driven priors [12, 32]. However, despite these impressive developments, obtaining full spatial 3D understanding of a whole scene still remains an extremely challenging task.

On one hand many approaches aim to estimate 3D geometry directly from visual data, for instance by predicting mesh geometry [40, 12, 5], voxel grids [6, 10, 41, 42] or using implicit surface functions [27, 30]. On the other hand, another line of research leverages object priors from 3D CAD models datasets [17, 15, 20, 38]. Their main idea is to formulate image understanding as a joint detection and retrieval problem, where reconstruction relies on nearest neighbor retrieval of 3D models from the dataset. This leads to a simpler, lighter weight model architecture compared to methods directly predicting 3D geometry, and can even provide higher fidelity.

However, this direction often reaches limitations when only considering a single image as it is quite difficult to resolve the ambiguity of an object's depth and scale, and to

*First two authors contributed equally.
[1]Project page: http://www.kmaninis.com/vid2cad

infer spatial arrangements among objects only with learnt priors from 2D input. The ambiguity arises because there are many combinations of an object's depth and scale (size) values that lead to the same projection on the image (e.g., large but far away from the camera, or small but near the camera). In this work, we argue that it is sensible to relax the task and utilize a sequence of RGB images since many computer vision application are not limited to a single image, but can rather rely on a video stream. While performing the task of 3D scene understanding on videos instead of single RGB images seems more tractable at a first glance, it raises the question of how to efficiently integrate the per-frame predictions of neural networks.

In this paper, we address the question of how to integrate 3D shape retrievals and alignments from individual frames, e.g., obtained by Mask2CAD [20], over a series of video frames in order to produce a globally-consistent 3D representation of the whole scene. We propose Vid2CAD, which leverages multi-view consistency constraints to resolve scale and depth ambiguities. Our key observation is that the ambiguity can be resolved with constraints on the projections on multiple views, as the object size must remain constant across all of them. We feed the per-frame object pose predictions into a temporally global non-linear least squares formulation which integrates them across views in order to reconstruct the absolute scale and depth of the retrieved object. This temporal aggregation process also improves the estimates of other pose parameters such as the object's 3D rotation, and the x,y coordinates of its 3D center. Finally, by leveraging multi-view constraints our method resolves occlusions and handles objects that are out of view in individual frames, thus reconstructing all objects in the scene into a single globally consistent 3D representation. In summary, given a video, our method automatically recovers the shape and full 9 DoF pose of each object appearing in it (3D rotation, 3D translation, and scaling along all 3 axes).

We perform extensive experiments on the challenging Scan2CAD dataset [1] which features videos of complex indoor scenes with multiple objects. In comparison to the state-of-the-art single-frame method Mask2CAD that we build on, we achieve a substantial improvement with our temporal integration (from 11.6% to 30.2% class average accuracy).

2. Related Work

3D from a single image. Many works in this area [40, 27, 6, 10, 41, 42, 30, 5] reconstruct a single object appearing at a fixed 3D position, depth, and scale (i.e., only shape and rotation vary). Several recent works consider scenes with multiple objects, typically by first detecting them in the 2D image, then reconstructing their 3D shape and pose [15, 12, 20, 17, 39, 19, 28, 32]. These works compensate for the scale-depth ambiguity in variety of ways, e.g., based on estimating an approximate pixelwise depth map from the input image [15], by requiring manually provided objects' depth and/or scale [12, 20] at test time, or by estimating the position of a planar floor in the scene and assuming that all objects rest on it [17]. A few works [39, 28] even attempt to predict object depth and scale directly based on image appearance (which makes them dependent on implicit contextual cues in the overall room appearance). Finally, CoReNet [32] directly predicts a global 3D scene volume containing all objects in one pass. However, it has been demonstrated only on scenes with 2 or 3 objects and the monolithic nature of the model makes it unlikely to generalize to more objects.

Our method is mostly related to works based on retrieving the most similar rendering of a CAD model to a 2D detection [17, 15, 20], out of a given CAD database. This provides the object's shape and 3D rotation, as well as the x,y coordinates of its center. We propose to resolve for the depth and scale parameters with multi-view integration.

3D from multiple views. Classical works reconstruct a 3D point cloud from multiple views of a scene based on keypoint correspondences [31, 36]. However, the output point cloud is not organized into objects with their semantic labels, 3D shapes, or poses. Very recently FroDO [35] extended this line of works by also detecting objects and reconstructing them in 3D, using both 2D image cues as well as the 3D point cloud. We tackle the same task, but propose different multi-view consistency constrains, have a simpler system that does not require reconstructing 3D point clouds, and show a quantitative evaluation on scenes with multiple objects (ScanNet [7], only qualitative in [35]).

Finally, the recent [33] reconstructs the shape of a single object given two calibrated views with a neural network.

Aligning CAD models to RGB-D scans. Several works propose techniques for 9 DoF object pose estimation by aligning CAD models to RGB-D scans, generated by fusing RGB-D video frames into a high-quality, dense 3D scans for the scene [22, 1, 2, 16]. These methods have access to much more and cleaner information than our method does, but are limited to videos acquired by an RGB-D sensor. An important advantage of requiring only RGB videos is that it opens up the possibility of operating on a much larger pool of videos, e.g. from YouTube, without constraints.

3. Method

Our goal is to align clean CAD models from a database to a video of a scene (Fig. 1). For each object, we want to find which CAD model corresponds to it, and a 9 Degrees-of-Freedom (DoF) transformation that maps from its initial database pose to the 3D world (scene). We seek for a 3 DoF rotation matrix R, a 3 DoF translation vector t, and a 3 DoF anisotropic scaling vector $s = (s_x, s_y, s_z)^T$ such that

t	3×1 translation CAD $\rightarrow$ world
R	3×3 rotation CAD $\rightarrow$ world
s	3×1 scaling CAD $\rightarrow$ world
i	frame index
R^i	3×3 rotation CAD $\rightarrow$ camera view space
s^i	3×1 scaling CAD $\rightarrow$ world
E^i	3×4 extrinsic camera matrix
E^i_R, e^i_t	3×3 rotation and 3×1 translation of E^i.
K^i	3×3 intrinsic camera matrix
$\hat{c}^i$	2×1 object center in the image
$\hat{b}^i$	2×1 amodal box in the image
β^i	1×1 depth value of the object center

Table 1: Math notation. The first three rows determine the 9 DoF object pose we want to reconstruct. We use the superscript ^{i} for entities attached to frame i, and $\hat{}$ for 2D vectors on an image.

the vertices v of the CAD model are placed in their correct position in the world by applying the transformation:

$$h(v) = t + R \cdot s \cdot v \tag{1}$$

The CAD models live in a canonical space in the database (scale-normalized to a constant size, centered at the origin, and in a canonical orientation common to all objects within a class). We assume that we know the pose of the camera w.r.t the world at each video frame i (extrinsic calibration matrix $E^i = [E^i_R | e^i_t]$) as well as the projection function to the image (intrinsic calibration matrix K^i). The object projects to image i by $\hat{v}^i = K^i \cdot (e^i_t + E^i_R \cdot h(v))$. Tab. 1 summarizes our notation.

In Sec. 3.1, we first review how the task can be (partially) addressed given a single image by the state-of-the-art method Mask2CAD [20]. We discuss its shortcomings and then propose a solution that leverages multi-view constraints induced by the video (Sec. 3.2). In Sec. 3.3, we discuss an extension involving predicting approximate object scale from a single frame based on recognition.

3.1. Base method: Mask2CAD

The technique. Mask2CAD [20] is based on a semantic instance segmentation model [23, 13], which detects objects of a predefined set of classes in an image i. For each detection, Mask2CAD predicts 2D properties (i.e., 2D bounding box, class, confidence score, and segmentation mask), as well as some 3D properties: rotation R^i, the 2D projection $\hat{c}^i \in \mathbb{R}^2$ of the 3D center on the image, and a shape code vector f^i. The latter is used to compare natural images of objects to synthetic images of the CAD models. During inference Mask2CAD retrieves the most similar CAD model from the database based on similarity in an appearance embedding space. This CAD model is then placed in the world by using the predicted rotation R^i, while translating the object by moving the predicted center $\hat{c}^i$ to a manually-given

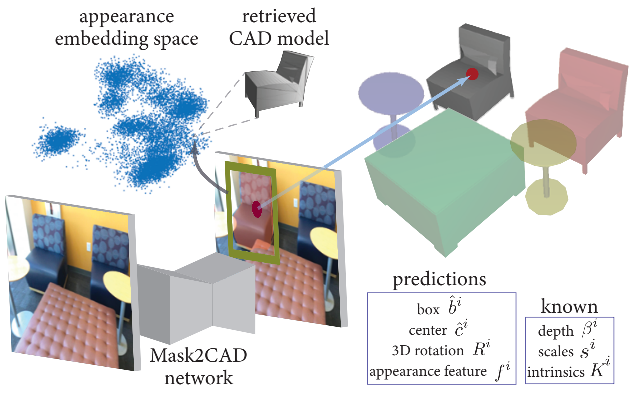

Figure 2: **The Mask2CAD method:** On top of the traditional 2D instance segmentation outputs (box, class, mask), Mask2CAD predicts the 2D projection $\hat{c}^i$ of the 3D object center on the image, the 3D rotation matrix R^i, and the shape code vector f^i, but requires the depth β^i of the center and the scaling transformation s^i as labeled input.

depth value β^i by using the intrinsic matrix K^i (Fig. 2). The size of the object is also manually provided through the known vector s^i.

Strengths and limitations. As Mask2CAD casts 3D object reconstruction as retrieval of clean CAD models, it naturally outputs high-quality shapes, without the need to address over-smoothing or tessellation artifacts typical of methods that predict 3D geometry directly from the image (e.g., voxel grids [6, 10, 41, 42], meshes [40, 12, 5] or point clouds [9, 25]).

However, given a single image, Mask2CAD is not able to infer the size of the objects nor their position along the z axis (depth β), due to the scale-depth ambiguity. The ambiguity arises because of the projection from 3D to 2D (Fig. 3, left). By simultaneously changing the size of an object and its position along the depth axis, we can obtain the same projection on the image (e.g., a small object near the camera, or a large object far from it). This scale-depth ambiguity is an inherent limitation for 3D reconstruction methods from a single image, which need to compensate for it in various ways (Sec. 2).

In practice, Mask2CAD as well as Mesh-RCNN [12] work around this limitation by using the ground-truth depth β^i and the size of the objects during inference (as the database-to-world scaling transformation s^i). In real settings, this information is not available at test time and such methods are not usable automatically.

3.2. Temporal integration

We propose to integrate the single-frame Mask2CAD predictions across frames in a video, as they offer multiple views of the same objects. This integration process brings several advantages: (1) it resolves the scale-depth ambiguity, inferring both of them automatically (Fig. 3, right); (2)

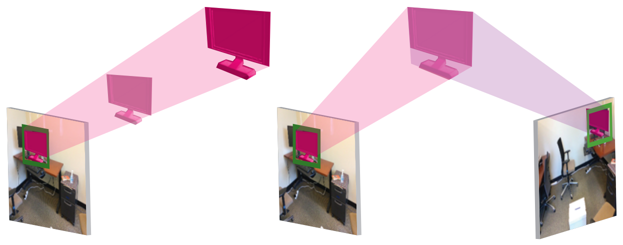

Figure 3: **Scale-depth ambiguity:** (Left) Placing a small object near the camera or a larger copy of the same object far from it lead to the same projection on the image. (Right) We address this by leveraging multiple views constraints.

it improves the estimates of other pose parameters such as the object's 3D rotation, and the x,y coordinates of its 3D center; (3) it resolves occlusions and objects that are out of view in individual frames, allowing to create one globally consistent 3D reconstruction of the scene (rather than a separate partial reconstruction for each frame).

Different video frames offer different views of the same scene and thus different constraints on the translation t, rotation R, and scaling s transformations of an object. We formulate temporal integration as an optimization problem, applied to one object at a time. For each video frame i, our method inputs the Mask2CAD predictions for that object in frame i, i.e., rotation R^i, 2D projection $\hat{c}^i$ of center, shape code f^i, and 2D bounding box $\hat{b}^i$. We output a single integrated CAD model selection and a full 9 DoF pose (t, R, s) mapping it to the world. Below we explain how we do it.

Selecting a CAD model. Each frame votes with its predicted shape code vector f^i, with weight proportional to the object detection score of Mask2CAD in that frame. We select the CAD model with the highest vote.

Optimization formulation. We use hard constraints as well as soft-constraint terms arising from relaxing multi-view geometric constraints imposed by relating a single desired output pose to multiple predictions from the individual frames (which are naturally noisy). In the following we present the terms (3), (4), (6), (8) separately first, and then combine them into our overall optimization objective (9).

Constraints for translation t. The 3D object center must project near the 2D centers $\hat{c}^i$ predicted by Mask2CAD in each frame, thus inducing multi-view constraints for the object translation t (Fig. 4). All CAD models are pre-processed, so that they are centered at the origin of their canonical space. Applying (1) for objects at the origin, instead of a variable object center, removes the dependency of the center on rotation R and scaling s. Hence, the object center in world space becomes equal to t:

$$t + R{\cdot}s{\cdot}(0,0,0)^T = t + (0,0,0)^T = t \tag{2}$$

To create the constraints, we model the object center as seen from each frame i using 3 auxiliary variables – the 2D position in image space $\hat{\kappa}^i = (\hat{\kappa}^i_x, \hat{\kappa}^i_y)$ and the depth β^i with respect to frame i (Fig. 4, right). We add a soft-constraint that keeps $\hat{\kappa}^i$ close to the 2D center $\hat{c}^i$ predicted by Mask2CAD. We transform $(\hat{\kappa}^i_x, \hat{\kappa}^i_y, \beta^i)$ to world space and add another soft constraint that keeps the resulting constructed 3D center close to the desired object center t (which we are looking for). Therefore, the 2D center objective $l^i_{\hat{\kappa}}$ and the 3D translation objective l^i_t are:

$$l^i_{\hat{\kappa}} = \left\| \hat{\kappa}^i - \hat{c}^i \right\|_{L_1} \tag{3}$$

$$l^i_t = \left\| (E^i_R)^{-1}(K^i)^{-1}{\cdot}(\beta^i\hat{\kappa}^i_x, \beta^i\hat{\kappa}^i_y, \beta^i)^T - e^i_t - t \right\|_{L_1} \tag{4}$$

In our overall objective, we will minimize (3) over $\hat{\kappa}^i$, while minimizing (4) over β^i, $\hat{\kappa}^i$, and t. Thus, we need multiple frames to avoid degenerate solutions for t.

Modeling centers per-frame simplifies the projection equations and improves reconstruction performance compared to projecting the 3D object center t to all frames and comparing to $\hat{c}^i$ directly. In the latter case, frames where the object is close to the camera get a large weight due to the division by a small depth value during projection. Modeling the 2D object centers as separate variables $\hat{\kappa}^i$ solves this issue, allowing us to add a hard constraint that keeps them above a minimum depth in each frame: $\beta^i > 0.1$m.

Constraints for rotation R. To create constraints for R, we note that there are two ways to transform the object from database space to the 3D coordinate system of the camera in a frame i (camera view space): (1) move the object into world space through the 9 DoF pose transformation (t, R, s) and then into camera view space through the extrinsic parameters E^i; or (2) directly use the rotation matrix R^i predicted by Mask2CAD from frame i and combine it with the translation vector t^i from database space to camera view space. Both ways lead to the same result:

$$e^i_t + E^i_R{\cdot}(t + R{\cdot}s{\cdot}v) = t^i + R^i{\cdot}s{\cdot}v \tag{5}$$

This equation is valid for any point on the object. Assuming non-degenerate transformations, this can only be true if $E^i_R{\cdot}R = R^i$. We use this to create a soft constraint, the rotation objective l^i_R for each frame:

$$l^i_R = \left\| R^i - E^i_R{\cdot}R \right\|_{L_2} \tag{6}$$

We ensure R remains a valid rotation matrix during the optimization process by adding a hard constraint keeping its corresponding quaternion normalized.

For vertically symmetric objects, we look for any valid rotation by considering only the minimum distance of the predicted rotation to all valid rotations in the objective (6).

Constraints for scaling s. To infer the anisotropic scaling transformation s, and thus the size of the objects in 3D, we use the 2D amodal bounding boxes $\hat{b}^i$ predicted by Mask2CAD (Fig. 4). Since the scaling affects the projection

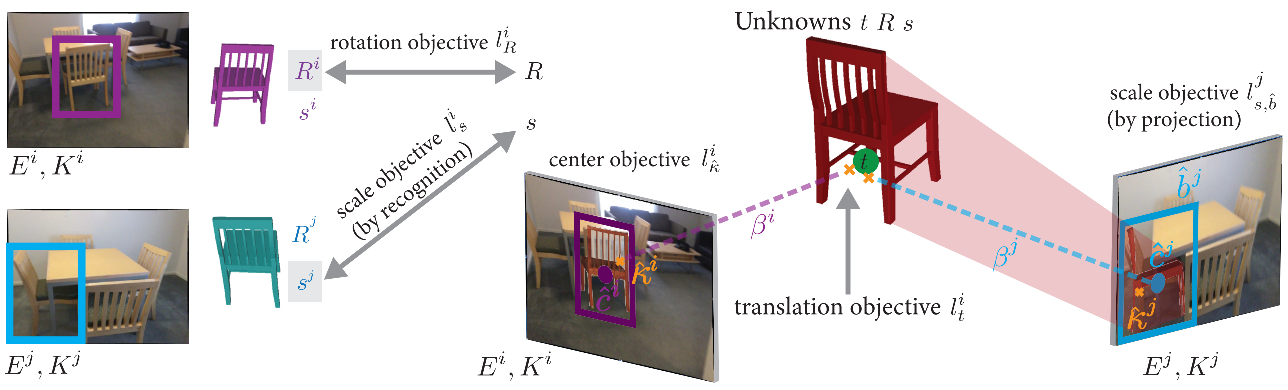
rotation objective l_R^i
R^i
s^i
R
s
scale objective l_s^i (by recognition)
R^j
s^j
E^i, K^i
E^j, K^j
Unknowns t R s
center objective $l_{\hat{\kappa}}^i$
β^i
β^j
$\hat{\kappa}^i$
$\hat{c}^i$
translation objective l_t^i
scale objective $l_{s,\hat{b}}^j$ (by projection)
$\hat{b}^j$
$\hat{c}^j$
$\hat{\kappa}^j$

Figure 4: **Temporal Integration:** We formulate our task as a constrained optimization problem with objectives that arise from multi-view constraints, given by the input frames (left). The center objective (3) keeps the value of the auxiliary variable $\hat{\kappa}^i$ close to the predicted box center $\hat{c}^i$ in frame i (center of figure). The translation objective (4) maintains the consistency between the desired 3D object center t and the center $(\hat{\kappa}_x^i, \hat{\kappa}_y^i, \beta^i)$ formed by the auxiliary variables and the desired depth β^i. The rotation objective (6) relates the desired rotation R to the rotations R^i predicted in each frame (top-left image). Finally, the scale objectives (8), (10) constrain the desired scaling transformation s based on the predicted box ($\hat{b}^j$ in the right image) and the predicted scalings s^i (bottom-left image), respectively.

of the CAD model vertices on the image, we design constraints so that s leads to projections respecting these boxes. Specifically, for a candidate value of s, we first project the vertices v of the CAD model on frame i based on s:

$$\hat{v}^i = K^i \cdot \left(e_t^i + E_R^i \cdot (t + R \cdot s \cdot v)\right) \tag{7}$$

We apply this transformation to all vertices and compute the bounding box $\hat{v}_{box}^i$ around the resulting 2D points $\hat{v}^i$. Then, we soft-constrain this box to match $\hat{b}^i$, resulting in the objective:

$$l_{s,\hat{b}}^i = \mathrm{d}_{\mathrm{box}}(\hat{v}_{box}^i, \hat{b}^i) \tag{8}$$

where $\mathrm{d}_{\mathrm{box}}$ is the L_1 distance between the box sides (left, right, top, bottom). In addition to the unknown s, this objective also depends on other unknowns R, t. During optimization, we jointly solve for all unknowns simultaneously.

Overall optimization objective. The full objective l^i for frame i is formulated as a weighted sum of the objectives above, and the total sum over all frames is:

$$L = \sum_i l^i = \sum_i a_t l_t^i + a_{\hat{\kappa}} l_{\hat{\kappa}}^i + a_R l_R^i + a_{s,\hat{b}} l_{s,\hat{b}}^i \tag{9}$$

We jointly minimize the objective L over the desired 9 DoF transformation (R, t, s), as well as over the auxiliary variables $\hat{\kappa}^i$ and β^i that we introduced. The optimization is subject to the two hard constraints we formulated above (i.e., $\beta^i > 0.1m$ and the rotation quaternion normalization). The objective function has L1 and L2 terms in the variables being optimized, which we optimize using gradient descent (initialized with $t = (0,0,0), s = (1,1,1)$, identity rotation R, $\hat{\kappa}^i$ to the center of the image, and $\beta = 1m$). We set the hyper-parameter weights a empirically.

3.3. Predicting object scale from a single frame

Scale from recognition. Due to the scale-depth ambiguity one cannot determine the 3D scale and depth of an *arbitrary* object from a single image. However, if the object class is known, one can use the average class size as a rough estimate [43]. We can go a step further by noticing that the size of an object depends on its particular model within a class, which can be estimated based on its 2D appearance alone, i.e., by recognition. We exploit this by augmenting Mask2CAD with a head to directly predict the scaling factor s mapping the CAD model to the world, for each detected box. For better results, we use a separate scale regressor specialized for each class. Notice that basic Mask2CAD already predicts a class for each box, which we use to select which regressor output to take.

Using single-frame scale in temporal integration. Predicting object scales by recognition can benefit temporal integration. We add to (9) a term encouraging the output object scaling s to be close to the scalings s^i predicted in the individual frames:

$$l_s^i = \left\| s - s^i \right\|_{L_1} \tag{10}$$

Note that inferring scalings within our temporal integration method based on projection on amodal 2D boxes (8) or based on recognition (10) are complementary and work best when used together (Sec. 4.2).

Deriving object depth from a single image. By having a prediction s for the size of the object from a single frame, we can also infer the depth of the object by minimizing the reprojection error of the CAD model on the predicted amodal 2D bounding box (analog to (8), but this time optimized over depth). A related technique was also presented in [19]. While in theory this trick addresses the scale-depth ambiguity even from a single frame, in practice the estimated depth values are quite unstable, as they are strongly affected by small inaccuracies in the predicted amodal box, object scale, predicted rotation, and/or predicted object center. As we show in Sec. 4, quantitative results are much better when using temporal integration.

3.4. Implementation details

Mask2CAD architecture. We use the default settings for the network architecture, which builds on the ShapeMask [21] instance segmentation method with ResNet-50 [14] backbone. For the added scale prediction branch we used 4 convolution blocks with a fully-connected output layer that outputs $3 \cdot N_{cls}$ outputs for the class-specific anisotropic scalings (with N_{cls} the number of classes).

Temporal association. Our temporal integration method (Sec. 3.2) takes as input the predictions of Mask2CAD for one object across multiple frames. However, Mask2CAD detects objects independently in each frame. Hence, we first automatically associate detections across frames using a tracking-by-detection approach (Sec. 4.2 in [26]).

Each output track collects the per-frame detections for one physical object, on which we apply our method.

Some objects go out of view and re-appear later on, causing fragmented tracks. We fix this issue by clustering in 3D world space the object alignments produced by our temporal integration method from the initial tracks. Then we merge tracks within a cluster (which typically correspond to the same physical object) and run again our temporal integration process on the merged tracks. This improves the estimated 9DOF pose of the objects as the second temporal integration sees more views of the same object at once.

4. Experiments

We perform extensive experimental evaluation on Scan2CAD [1], which provides ground truth CAD annotations on top of ScanNet [7]. We first evaluate Mask2CAD as a single-frame baseline in Sec. 4.1. We then evaluate our full temporal integration and present an ablation study of its individual components in Sec. 4.2.

Datasets and evaluation metric. We use videos from ScanNet [7], 3D CAD models from ShapeNetCore [3], and annotations that connect the two from Scan2CAD [1]. ScanNet provides RGB-D videos of rich indoor scenes with multiple objects in complex spatial arrangements. It also provides camera parameters for individual frames and dense depth fusion [29, 8] reconstructions. *We only use the RGB videos and the camera parameters, ignoring all depth data.* ShapeNetCore provides CAD models from 55 object classes, in a canonical orientation within a class. Scan2CAD provides manual 9 DoF alignments of ShapeNet models onto ScanNet scenes for 9 super-classes.

We use these data sets both for training and for evaluation. During training, we consider all ScanNet videos in the official train split whose scenes have Scan2CAD annotations (1194 videos). For training the Mask2CAD network, we take individual video frames and we project the aligned CAD models onto them. We set the weights a of the optimization objective (9) empirically on the same training set.

We evaluate our method and the baselines on the 312 videos in ScanNet's val split. We quantify performance using the Scan2CAD evaluation protocol [1]: a ground-truth 3D object is considered accurately detected if one of the model outputs matches its class and 9 DoF alignment (within error thresholds: 20% scale, 20° rotation, 20cm translation). We report accuracy averaged over classes ('class avg.') as well as over all object instances ('global avg'). The val set contains 3184 objects.

Training Mask2CAD. We train Mask2CAD for 96000 iterations with the same data augmentations as in [20] (HSV-color, ROI, and image scale jittering). The initial learning rate is set to 0.8 and is reduced by a factor of 10 at $2/3$ and $5/6$ of the total number of iterations. We include objects that are partially visible and whose center is truncated during training, as it improves performance.

4.1. Single-frame baselines - Mask2CAD

Original Mask2CAD. We evaluate several variants of our single-frame Mask2CAD baseline. The first one (b_1) is the setting from the original paper [20] and uses ground-truth depth and object size at test time to tackle the scale-depth ambiguity. It also relies on the ground-truth 2D object boxes at test time. For each ground-truth box we only keep the most overlapping detected box (if it overlaps > 0.3). All other detections are discarded. We call this procedure 'ground-truth association'. We also discard all detections with a low score < 0.2. This model is directly given 4 out of the 9 DoF as ground-truth at test time (1 depth and 3 scales). It also benefits from the cleanup made by ground-truth association, which indirectly provides some information about 2 other DoFs (x,y coordinates of the center). Having access to this much ground-truth at test time is unrealistic. In the following we explore several variants of Mask2CAD which use less of it.

More automatic variants. As variant b_2, we estimate an object depth and scale by taking the average scale and depth of its class from the training set. This does not require altering Mask2CAD's architecture.

An arguably better way to estimate scale and depth automatically is our idea from Sec. 3.3: we extend MaskCAD's architecture to predict object scale and then use it to derive depth by reprojection on the 2D box (variant b_4).

For both ways to get scale and depth we consider using ground-truth association or not. In the latter case detections

Family	id	depth	scales	association	rot. sym.	**class avg.**	**global avg.**	bathtub	bookshelf	cabinet	chair	display	sofa	table	trashbin	other
Single-frame baselines	b_1	gt	gt	gt	-	33.7	41.2	24.2	25.0	24.2	68.9	48.2	31.9	28.9	48.7	3.4
	b_2	avg	avg	gt	-	2.5	3.8	0.0	1.9	1.5	7.7	4.7	1.8	1.4	2.6	1.2
	b_3	avg	avg	thr	-	2.5	3.5	0.0	1.9	1.5	6.8	3.7	2.7	1.4	3.0	1.2
	b_4	deriv	pred	gt	-	12.1	16.9	9.2	2.8	6.9	33.2	17.3	6.2	7.2	25.4	0.5
	b_5	deriv	pred	thr	-	11.6	16.0	8.3	3.8	5.4	30.9	17.3	5.3	7.1	25.9	0.5
Temporal Integration	F	mv	mv+pred	track	yes	30.2	38.4	27.5	12.3	23.5	65.5	35.1	24.8	27.7	50.4	5.4
	a_1	mv	mv	gt	no	33.5	41.0	25.8	20.8	30.4	65.6	26.7	33.6	35.1	60.8	2.7
	a_2	mv	pred	gt	no	30.2	38.0	25.0	15.6	20.4	65.8	40.8	19.5	23.3	58.6	2.4
	a_3	mv	mv+pred	gt	no	37.4	44.9	38.3	17.9	33.5	73.3	39.8	32.7	31.5	63.4	6.1
	a_4	mv	mv+pred	gt	yes	37.6	45.2	38.3	17.9	33.5	73.3	39.8	32.7	32.2	64.7	6.1

Table 2: Quantitative evaluation on the Scan2CAD dataset [1]. We compare single-frame baselines (b) to our multi-view integration method (F and a). Method b_5 is the best fully automated single-frame baseline, and F is our fully automated temporal integration method. The shortcuts are: ground-truth (gt), average (avg), predicted (pred), derived based on scale and reprojection (deriv), estimated based on multi-view constraints (mv). See main body text for details.

are simply filtered at 0.2 score, which leads to fully automatic models b_3, b_5.

Duplicate removal. Detections for the same physical object in different frames result in multiple copies in the output, which might lower the performance metrics for these single-frame baselines. Hence, we use our 3D clustering algorithm from Sec. 3.4 to remove such duplicate detections (i.e., keeping only the top-scored one in each cluster).

Results (Tab. 2). Model b_1 achieves 33.7% accuracy, which can be seen as a theoretical upper bound of Mask2CAD as it uses substantial ground-truth information at test time. Using class-average depth and scale values instead of ground-truth leads to poor results, reaching only 2.5% accuracy for models b_2, b_3. This is not surprising, as the evaluation metric demands rather accurate poses. Our extension from Sec.3.3 allows to predict object depth and scale by recognition, improving performance substantially to 12.1% (b_4) and 11.6% (b_5). The difference due to using ground-truth association is small (0.5% from b_4 to b_5). Model b_5 represents the best fully automatic variant of Mask2CAD we built, and is the reference model to improve further upon with temporal integration.

4.2. Temporal integration

Our fully-automated method. Our full temporal integration method F uses all objective function terms (9) and (10), and performs temporal association with a tracker (Sec. 3.4). It is fully automatic as it does not use any ground-truth at test time. It achieves 30.2% accuracy, 2.6× better (+18.6%) than the best automatic single-frame method b_5 (which already included our enhancements from Sec. 3.3). These comparisons demonstrate the dramatic improvements brought by our main contribution. We show qualitative results in Fig. 5.

Ablation study. We study the effect of varying the way we estimate object scale during temporal integration, and the use of a rotation symmetry term. This results in 4 settings (a_1-a_4) and we show their performance in Tab. 2.

The first way (a_1) is to estimate scale based only on multi-view reprojection constraints (8) on 2D detection boxes. The second way (a_2) is to only use the single-frame Mask2CAD scale predictions via the term (10). The first way performs better by +3.2%, highlighting the power of multi-view constraints. Moreover, using both ways (a_3) improves accuracy further by +3.9%, showing that the two mechanism are complementary. Finally, taking into account vertically symmetric objects (a_4) as described in Sec. 3.2 improves only by a small amount (+0.2%).

For this ablation we used ground-truth association instead of the automatic tracker. As in Sec. 4.1, this matches detections to ground-truth boxes and it brings perfect temporal association (via the 3D object id associated to a box in the annotations of Scan2CAD). This keeps the study focused on the differences brought by the various terms in our core method, removing secondary effects due to the tracker and our track merging mechanism (Sec. 3.4). It also allows to estimate the margin for improvement when using better tracking algorithms: a_4 is only moderately better than our fully-automatic method F (+7.4%). Finally, a_4 can be fairly compared to single-frame baseline b_4, as they both use the same ground-truth association. Our temporal integration brings massive improvements also in this case (+25.5%).

Comparing to methods using RGB-D scans. For reference, we also compare to methods [2, 1] that input high-quality dense 3D scans obtained by depth-fusion from RGB-D videos. Those have an advantage as they have access to the 3D scene geometry and operate by directly fitting CAD models to it. Surprisingly, our fully automatic method

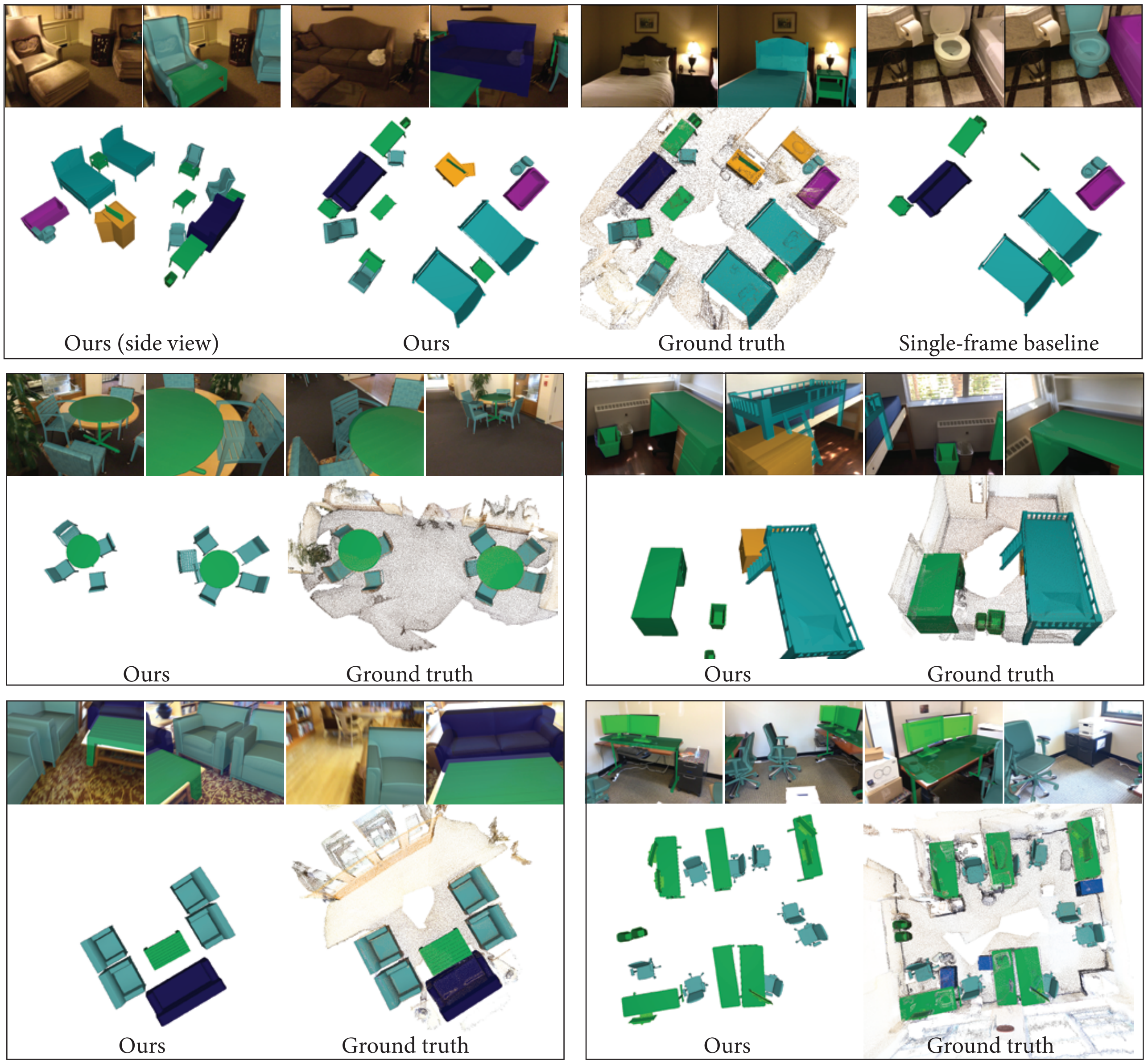

Figure 5: **Qualitative results:** We compare the alignment produced by our temporal integration method to the ground-truth and to the best automatic single-frame baseline (top); i.e., our extended Mask2CAD, cf. Tab. 2, b_5. We also show our alignments overlaid on the input frames, which highlight the difficulty of the problem as only a small part of the scene is visible in each frame.

F performs on par with [1] (35.6% class avg, 31.7% global avg; vs our 30.2%/38.4%, Tab. 2). While the state-of-the-art [2] performs even better (44.6%/50.7%), this family of methods are limited to videos acquired by RGB-D sensors, whereas our method can work on any RGB video.

5. Conclusions

We have introduced Vid2CAD, a method to align CAD models to a video sequence of complex scenes containing multiple objects. Our core idea is to integrate per-frame network predictions across time by leveraging multiple-view constraints, thus obtaining a globally-consistent 3D scene represented by the underlying CAD models. Compared to the best single-frame method Mask2CAD, our temporal integration achieves a substantial improvement, from 11.6% to 30.2% class average accuracy. Overall, we consider our method a first stepping stone towards 3D scene understanding on video sequences using CAD model abstractions as priors. For instance, we could see extensions towards joint camera poses estimation or semantic scene understanding; however, particularly in dynamic environments, we believe that a CAD-based scene representation can serve as a reliable important prior to understand the environment.

Acknowledgements: We thank Weicheng Kuo for providing us with detailed information about Mask2CAD, and for helping us to train and evaluate it. We thank Angela Dai for her contribution in the supplemental video. This work was supported by the ERC Starting Grant Scan2CAD (804724).

References

[1] A. Avetisyan, M. Dahnert, A. Dai, M. Savva, A. X. Chang, and M. Nießner. Scan2CAD: Learning cad model alignment in rgb-d scans. In *CVPR*, 2019. 2, 6, 7, 8

[2] A. Avetisyan, A. Dai, and M. Nießner. End-to-end cad model retrieval and 9dof alignment in 3d scans. In *ICCV*, 2019. 2, 7, 8

[3] A. X. Chang, T. Funkhouser, L. Guibas, P. Hanrahan, Q. Huang, Z. Li, S. Savarese, M. Savva, S. Song, H. Su, et al. Shapenet: An information-rich 3d model repository. *arXiv:1512.03012*, 2015. 6

[4] L.-C. Chen, G. Papandreou, I. Kokkinos, K. Murphy, and A. Yuille. DeepLab: Semantic image segmentation with deep convolutional nets, atrous convolution, and fully connected CRFs. *TPAMI*, 2018. 1

[5] Z. Chen, A. Tagliasacchi, and H. Zhang. Bsp-net: Generating compact meshes via binary space partitioning. In *CVPR*, 2020. 1, 2, 3

[6] C. B. Choy, D. Xu, J. Gwak, K. Chen, and S. Savarese. 3D-R2N2: A unified approach for single and multi-view 3D object reconstruction. In *ECCV*, 2016. 1, 2, 3

[7] A. Dai, A. X. Chang, M. Savva, M. Halber, T. Funkhouser, and M. Nießner. Scannet: Richly-annotated 3d reconstructions of indoor scenes. In *CVPR*, 2017. 2, 6

[8] A. Dai, M. Nießner, M. Zollhöfer, S. Izadi, and C. Theobalt. Bundlefusion: Real-time globally consistent 3d reconstruction using on-the-fly surface reintegration. *ACM Transactions on Graphics (ToG)*, 36(4):1, 2017. 6

[9] H. Fan, H. Su, and L. J. Guibas. A point set generation network for 3d object reconstruction from a single image. In *CVPR*, 2017. 3

[10] R. Girdhar, D. Fouhey, M. Rodriguez, and A. Gupta. Learning a predictable and generative vector representation for objects. In *ECCV*, 2016. 1, 2, 3

[11] R. Girshick. Fast R-CNN. In *ICCV*, 2015. 1

[12] G. Gkioxari, J. Malik, and J. Johnson. Mesh R-CNN. In *ICCV*, 2019. 1, 2, 3

[13] K. He, G. Gkioxari, P. Dollár, and R. Girshick. Mask R-CNN. In *ICCV*, 2017. 1, 3

[14] K. He, X. Zhang, S. Ren, and J. Sun. Deep residual learning for image recognition. In *CVPR*, 2016. 1, 6

[15] S. Huang, S. Qi, Y. Zhu, Y. Xiao, Y. Xu, and S.-C. Zhu. Holistic 3D scene parsing and reconstruction from a single RGB image. In *ECCV*, 2018. 1, 2

[16] H. Izadinia and S. M. Seitz. Scene recomposition by learning-based icp. In *CVPR*, 2020. 2

[17] H. Izadinia, Q. Shan, and S. M. Seitz. Im2CAD. In *CVPR*, 2017. 1, 2

[18] A. Krizhevsky, I. Sutskever, and G. E. Hinton. Imagenet classification with deep convolutional neural networks. In *NIPS*, 2012. 1

[19] A. Kundu, Y. Li, and J. M. Rehg. 3D-RCNN: Instance-level 3d object reconstruction via render-and-compare. In *CVPR*, 2018. 2, 5

[20] W. Kuo, A. Angelova, T.-Y. Lin, and A. Dai. Mask2CAD: 3D shape prediction by learning to segment and retrieve. In *ECCV*, 2020. 1, 2, 3, 6

[21] W. Kuo, A. Angelova, J. Malik, and T.-Y. Lin. Shapemask: Learning to segment novel objects by refining shape priors. In *ICCV*, 2019. 6

[22] Y. Li, A. Dai, L. Guibas, and M. Nießner. Database-assisted object retrieval for real-time 3d reconstruction. In *Computer Graphics Forum*, volume 34. Wiley Online Library, 2015. 2

[23] Y. Li, H. Qi, J. Dai, X. Ji, and Y. Wei. Fully convolutional instance-aware semantic segmentation. In *CVPR*, 2017. 3

[24] J. Long, E. Shelhamer, and T. Darrell. Fully convolutional models for semantic segmentation. In *CVPR*, 2015. 1

[25] P. Mandikal, N. K. L., M. Agarwal, and V. B. Radhakrishnan. 3d-lmnet: Latent embedding matching for accurate and diverse 3d point cloud reconstruction from a single image. In *BMVC*, 2018. 3

[26] M. J. Marin-Jimenez, A. Zisserman, M. Eichner, and V. Ferrari. Detecting people looking at each other in videos. *IJCV*, 106(3):282–296, 2014. 6

[27] L. Mescheder, M. Oechsle, M. Niemeyer, S. Nowozin, and A. Geiger. Occupancy networks: Learning 3d reconstruction in function space. In *CVPR*, 2019. 1, 2

[28] Y. Nie, X. Han, S. Guo, Y. Zheng, J. Chang, and J. J. Zhang. Total3dunderstanding: Joint layout, object pose and mesh reconstruction for indoor scenes from a single image. In *CVPR*, 2020. 2

[29] M. Nießner, M. Zollhöfer, S. Izadi, and M. Stamminger. Real-time 3d reconstruction at scale using voxel hashing. *ACM Transactions on Graphics (ToG)*, 32(6):1–11, 2013. 6

[30] J. J. Park, P. Florence, J. Straub, R. Newcombe, and S. Lovegrove. Deepsdf: Learning continuous signed distance functions for shape representation. In *CVPR*, 2019. 1, 2

[31] M. Pollefeys, R. Koch, and L. Van Gool. Self-calibration and metric reconstruction inspite of varying and unknown intrinsic camera parameters. *IJCV*, 32(1):7–25, 1999. 2

[32] S. Popov, P. Bauszat, and V. Ferrari. CoReNet: Coherent 3D scene reconstruction from a single rgb image. In *ECCV*, 2020. 1, 2

[33] N. Ravi, J. Reizenstein, D. Novotny, T. Gordon, W.-Y. Lo, J. Johnson, and G. Gkioxari. Accelerating 3d deep learning with pytorch3d. *arXiv preprint arXiv:2007.08501*, 2020. 2

[34] S. Ren, K. He, R. Girshick, and J. Sun. Faster R-CNN: Towards real-time object detection with region proposal networks. In *NIPS*, 2015. 1

[35] M. Runz, K. Li, M. Tang, L. Ma, C. Kong, T. Schmidt, I. Reid, L. Agapito, J. Straub, S. Lovegrove, et al. Frodo: From detections to 3d objects. In *CVPR*, 2020. 2

[36] J. L. Schonberger and J.-M. Frahm. Structure-from-motion revisited. In *CVPR*, 2016. 2

[37] K. Simonyan and A. Zisserman. Very deep convolutional networks for large-scale image recognition. In *ICLR*, 2015. 1

[38] M. Tatarchenko, S. R. Richter, R. Ranftl, Z. Li, V. Koltun, and T. Brox. What do single-view 3d reconstruction networks learn? In *CVPR*, 2019. 1

[39] S. Tulsiani, S. Gupta, D. Fouhey, A. A. Efros, and J. Malik. Factoring shape, pose, and layout from the 2d image of a 3d scene. In *CVPR*, 2018. 2

[40] N. Wang, Y. Zhang, Z. Li, Y. Fu, W. Liu, and Y.-G. Jiang. Pixel2mesh: Generating 3d mesh models from single rgb images. In *ECCV*, 2018. 1, 2, 3

[41] J. Wu, C. Zhang, T. Xue, W. T. Freeman, and J. B. Tenenbaum. Learning a probabilistic latent space of object shapes via 3D generative-adversarial modeling. In *NIPS*, 2016. 1, 2, 3

[42] H. Xie, H. Yao, S. Zhang, S. Zhou, and W. Sun. Pix2vox++: multi-scale context-aware 3d object reconstruction from single and multiple images. *IJCV*, 128(12):2919–2935, 2020. 1, 2, 3

[43] J. Y. Zhang, S. Pepose, H. Joo, D. Ramanan, J. Malik, and A. Kanazawa. Perceiving 3d human-object spatial arrangements from a single image in the wild. In *ECCV*, 2020. 5